Research Article | Vol. 30, No. 8 / 11 Apr 2022 / Optics Express 12427
Optics EXPRESS

Short single-frequency self-pulsing Brillouin-Raman distributed feedback fiber laser

REX H. S. BANNERMAN,[1,*] DEVIN H. SMITH,[2] ALAN C. GRAY,[1] JAMES C. GATES,[1] NEIL G. R. BRODERICK,[3] CORIN B. E. GAWITH,[1] AND PETER G. R. SMITH[1]

[1] *Optoelectronics Research Centre, University of Southampton, UK*
[2] *QuiX Quantum BV, Enschede, The Netherlands*
[3] *Dodd Walls Centre for Photonics and Quantum Technologies, Department of Physics, The University of Auckland, New Zealand*
[*] *r.h.bannerman@soton.ac.uk*

Abstract: We demonstrate that the stimulated Brillouin scattering of a 250 mm long distributed feedback Raman fiber laser can self-pulse with repetition rates up to 7 MHz, pulse widths of 25 ns, and peak powers of 1.2 W. While both CW and pulsed lasing are produced from a bespoke grating at 1119 nm this laser design could be constructed at almost any wavelength, as the Raman and Brillouin gain regions are relative to the pump wavelength. The laser has a low lasing threshold for a Raman laser of 0.55 W, a peak slope efficiency of 14 %, and a maximum average output of 0.25 W. An investigation of beating between pure Raman and Raman-pumped Brillouin lasing shows that the outputs of the two processes are highly correlated and thus the Brillouin lasing is essentially single-frequency when CW and near transform limited for pulsed operation. A phenomenological model of the Raman-Brillouin interaction shows that the pulsing behaviour of such a cavity is expected and produces very similar pulsing to that the seen in experimental results.

1. Introduction

Ultra-narrow linewidth lasers are a cornerstone of the current world of photonics. Due to their low phase and intensity noise, single frequency (SF) lasers are optimal for applications such as heterodyne detection, spectroscopy, and atomic laser cooling. An important class of SF lasers is based on π phase-shifted fiber Bragg gratings (FBG) that—due to their compact monolithic distributed feedback (DFB) structures—have a single longitudinal resonant cavity mode. π phase-shifted FBGs in erbium- or ytterbium-doped fibers can form SF lasers with single digit kHz linewidths, though only in the spectral gain band of the dopant [1,2], a major constraint. Atom cooling, for instance, requires SF lasers outside these regions for trapping and cooling atomic species such as rubidium (780 nm), calcium (657 nm), strontium (689 nm). Nonlinear frequency conversion is routinely used to generate laser at the cooling wavelengths from SF lasers such as erbium DFB fiber lasers using Second harmonic generation (SHG) to produce 780 nm for rubidium [3] or even fifth harmonic conversion for beryllium at 313 nm [4], but these routes are still limited to the harmonics of the spectral gain regions of rare earth ions. A good example are quantum memories using praseodymium which require SF lasers at 606 nm, a wavelength currently achieved using frequency stabilised dye lasers, and where there is not an appropriate rare-earth based source [5,6].

Rather than using population inversion in a lasing medium, as in conventional lasers, the whole field of Raman lasers uses Raman shifting of a pump laser in a Raman gain medium together with optical feedback to create a laser. These are comprehensively reviewed in a recent

#445876 https://doi.org/10.1364/OE.445876
Journal © 2022 Received 13 Oct 2021; revised 15 Jan 2022; accepted 16 Jan 2022; published 29 Mar 2022

Optics EXPRESS

book [7]. A key advantage of a Raman laser is that the spectrum of the gain is not reliant on the availability of an appropriate laser medium, but occurs at an energy offset from the pump (shifting light to longer wavelengths). Silica's Raman shift extends 16 THz below the pump frequency. The use of cascaded Raman shifting (for example using multiple Bragg gratings) allows a wide range of operating wavelengths [7]. While conventional Raman lasers use long lengths of fiber (typically 100s of meters), a special class of devices, which will be discussed in the background section, use π phase-shifted FBGs (also known as DFB Raman lasers). By resonating the Raman field in a high reflectivity Bragg grating cavity, much shorter lengths of fiber (tens of centimeters) can be used, and still obtain Raman-laser operation, and with the additional attraction of single-frequency operation. We believe that such lasers, when combined with efficient second harmonic generation in periodically poled nonlinear crystal waveguides, offer a versatile route to making narrow-linewidth and low-cost sources throughout the visible and near infra-red.

Surprisingly, when we built such a DFB Raman laser, we discovered that the stimulated Brillouin scattering (SBS) of the cavity-resonant stimulated Raman scattering (SRS) exhibits a novel self-pulsing behaviour resulting in laser pulses that were tens of nanoseconds long. This self-pulsing behaviour, if single frequency, is highly attractive for applications such as Doppler LIDAR [8] and more efficient frequency doubling [9].

2. Background

A π phase-shifted FBG based DFB Raman laser was first suggested by Youfang *et al.*, who theoretically predicted a subwatt lasing threshold and slope efficiency of >80 % [10]. Westbrook *et al.* demonstrated the first practical π phase-shifted FBG laser in highly nonlinear fiber at 1584 nm laser, but with a high threshold of 39 W [11]. By using a small-core fiber Shi *et al.* reduced the lasing threshold to 1 W, with a 1109.5 nm laser that had a maximum output power of 1.6 W [12]. A linearly polarised pump allowed them to improve the laser's performance, reporting a threshold of 440 mW, a slope efficiency of 13.5 % and a linewidth of <2.5 kHz [13].

Since then, much work has been done by Loranger *et al.*, who lowered the threshold to just 350 mW with lasers in the 1100 nm range as well as demonstrating DFB Raman lasers around 1550 nm [14–16]. Both Shi *et al.* and Loranger *et al.* claim the first observation of SBS of the resonant SRS and demonstrate that SBS emerges at higher pump powers than the SRS threshold, with Loranger *et al.* showing that the SBS clamps the SRS output power [14,17]. Loranger *et al.* hypothesised that the SBS was being amplified by a side passband of the FBG cavity, although to our knowledge no further work has been reported on this topic. Karpov *et al.* report seeing an active Q-switching burst pulse regime from a DFB mounted in a piezo tuneable tube, this laser produced microscecond bursts of nanosecond scale pulses when the piezo was resonantly driven and it is implied that these pulses are SBS [18]. There has also been reported work on π phase-shifted DFB pure Brillouin lasers [19,20], with one report even making a tantalising reference to Brillouin DFB lasers being "the basis for novel pulsed light sources" [7, p.237].

To the best knowledge of the authors, this is the first demonstration of self-pulsed SBS output from a π phase-shifted FBG. However, there are of course other laser configurations that show regular SBS self-pulsing. Pohl was the first to demonstrate passive SBS Q-switching in 1967 with both ytterbium glass and ruby rod lasers [21]. SBS self-pulsing in optical fiber was first reported by Harrison *et al.* in 1990 as chaotic pulsing, with their further reports showing periodic pulsing behaviours [22,23]. Since then, there has been much work on self-pulsing and self-Q-switching SBS fiber lasers pumped by rare-earth or multimode diodes in cavity lengths from meters to kilometers [24–30]. The laser presented here has a Raman cavity with a much shorter effective length of only about 50 mm, which is over an order of magnitude smaller than reported elsewhere for similar self-pulsed lasers.

Optics EXPRESS

3. Fabrication

The π phase-shifted FBG was fabricated using the small-spot direct UV Writing (SSDUW) technique [31]. This is a phase-controlled grating writing method that focuses two beams from the same CW 244 nm laser to a common focus forming an interferometric inscription pattern. The phase of the inscription pattern is computer controlled using an EOM present in one of the arms of the interferometer. The EOM is driven with nanometer-precise feedback from the 4-axis stage system below the writing interferometer atop which the fiber is mounted. The small spot size, here a diameter of 6 microns, along with the precise phase control allows for near-arbitrary gratings to be written [31]. The fiber is stripped and suspended between two clamps under a tension of 0.5 N. Coarse alignment is done visually and then the path of the suspended fiber's core is mapped in three axes using the fluorescence induced in the core by the laser which is attenuated by several orders of magnitude to limit exposure of the core.

To maximise the Raman gain Nufern's UHNA3 optical fiber was chosen due to its highly germanium doped core that has a radius of 1.8 microns. The resulting small mode field diameter of the fiber not only leads to a high Raman gain but also a high the Brillouin gain. Shi *et al.* used UHNA4, a near identical fiber with the only differences being a smaller core, marginally smaller mode field diameter, and a lower cut-off wavelength so performance should be comparable. The germanium content gives the fiber intrinsically high UV-sensitivity so hydrogen-loading is not required. The inscribed grating is 250 mm long with a uniform apodisation and a centrally located π phase shift to form the cavity structure. The grating's central wavelength of 1119 nm is within the germania Raman gain bandwidth, but detuned slightly from the peak at 1115 nm for UHNA4 when pumped by the 1064 nm laser used here, potentially resulting in slightly suboptimal Raman gain if UHNA3 has a similar gain spectra to UHNA4 [17]. A target grating coupling coefficient of $\kappa_{ac} = 30m^{-1}$ was used, which required 144 µW of UV laser power and writing speed of 45 mm min^{-1}; using such a low fluence means the UV induced losses are greatly reduce to the point of being negligible as compared to reflection or inherent propagation losses. The writing parameters were confirmed with a 10 mm test grating written physically and temporally before the cavity grating at a lower wavelength to limit interference from cladding modes. The

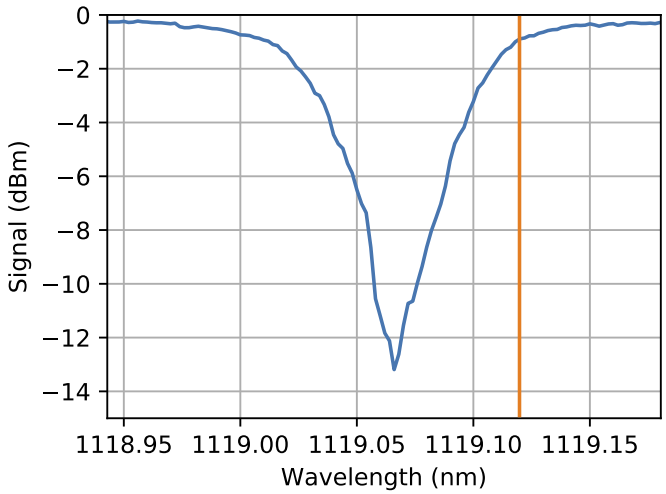

Fig. 1. Transmission spectra of the room temperature π phase-shifted DFB grating in UHNA3, limited by the OSA's resolution of 15 pm. The Brillouin shift of the cavity is shown with an orange line where a transmission of −1 dB is found, this is likely due grating side bands and therefore the Brillouin is likely bound in a highly lossy cavity.

Optics EXPRESS

gratings were measured in-situ both during and after fabrication in reflection and transmission using an OSA and a SLED centred at 1040 nm. The transmission spectrum of the DBR can be seen in Fig. 1, however the OSA's resolution of (15 pm) is insufficient to fully resolve both the grating, which should have a 3 dB bandwidth of 11 pm, and the cavity resonance, which has a sub-femtometer bandwidth. Ideally, a scanning Fabry–Pérot or tunable laser would be used to interrogate the cavity, but neither were available at this wavelength.

4. Results

The pulsed Raman laser setup is shown in Fig. 2, where the DFB grating was spliced onto Corning HI1060 fiber which was end-capped with 250 µm coreless termination fiber as a free-space pump was used. The grating section was mounted onto a copper bar, using polyamide tape at the ends of the bar, with thermal compound applied along the grating. This bar was clamped down onto an optical table with a small 2 mm spacer under the bar at the centre of the cavity. The small amount of bending by the spacer stabilises the laser behaviour in both CW and pulsed modes as it keeps the fiber in thermal contact with the bar.

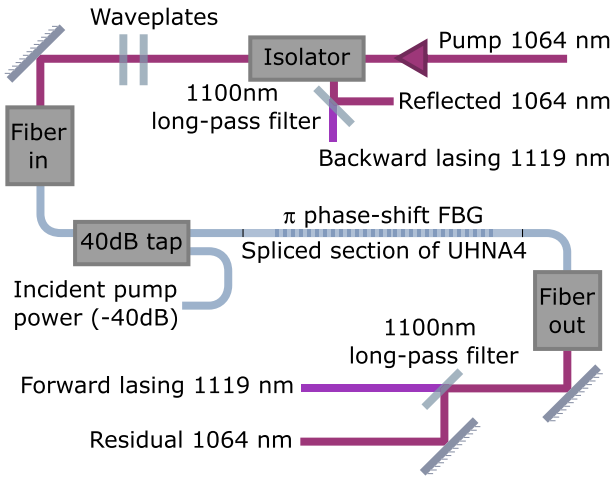

Fig. 2. Diagram of laser pump setup with free-space laser launch and filtering. Beam path is red for freespace and light blue for optical fiber.

To pump the laser a 1064 nm fiber laser from IPG was used, producing up to 10 W of highly stable 50 kHz linewidth linearly-polarised light. In the free-space launch waveplates are used to control the polarisation and any return light is recovered from the isolator, which is akin to using it as a circulator. A maximum coupling efficiency of the pump laser into the fiber of close to −3 dB was achieved, measured via a 40 dB fiber tap of incident pump power before the first HI1060 to UHNA3 splice. The splice loss between HI1060 and UHNA3 was found to be on average 0.9 dB. The output of the cavity was coupled to free space so a 1100 nm longpass edge filter could be used to separate the pump and lasing wavelengths. The residual pump and the forward lasing were coupled into optical fiber for characterisation using OSAs and fast (GHz) detectors.

Figure 3 shows the forward lasing power with respect to pump power, with the caveat that neither the incident pump nor the lasing output are corrected for splice loss. The lasing threshold was measured to be 550 mW with a maximum output power of 250 mW which was limited by available pump power. The peak slope efficiency of 14.0 % is essentially the same as the previous best of 13.5 % reported by Shi *et al.* [13]. It can be seen from Fig. 3 that there are regions of different slope indicating shifts in lasing operation above threshold. As the pulsing behaviour

Optics EXPRESS

begins less than 200 mW above the Raman lasing threshold, it is unlikely to be the direct source of the changing slope efficiency. While observing the laser spectrum on the OSA, particularly as the pump was altered, we began to suspect from the changing spectral shape, that more complex temporal effects were in play. Although little or no difference is seen in the average power between the CW and pulsed regimes.

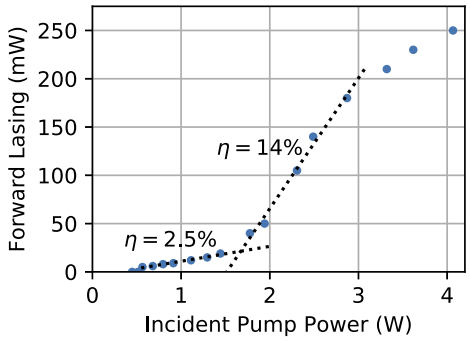

Fig. 3. Forward propagating output power of the laser, the saturation above 3 W is still under investigation.

To check the temporal characteristics, a fast InGaAs detector (PDA8GS: 750 - 1650 nm, DC - 9.5 GHz) and an Agilent 3 GHz oscilloscope were used to measure the temporal response and, dramatically, pulsing was observed. An example of the low-power pulsing behaviour is given in Fig. 4(a), showing the typical pulse shape expected from Q-switching, showing a smooth pulse with asymmetry as the pulse decays slower than it rises. The relationship of pump power to pulsing behaviour in Fig. 4(b) is also that expected of Q-switching with increasing pump power reducing the pulse-to-pulse period and pulse peak power being linearly proportional to the pump power. Another 1 GHz detector (1611FC-AC, 30 kHz - 1 GHz) was used to record the residual power temporal response in parallel with the laser output, with the two optical path lengths matched. As the residual power detector is AC-coupled calibration of power is challenging, so arbitrary units are given. Figure 5 shows the residual pump is depleted as Raman power builds up in the cavity, followed by a sharp rise when the pulse starts, fully recovering only after the pulse has finished. It should be noted that the OSA trace shows the average spectrum and does not allow us to determine whether there is a reduction in Raman output when the Brillouin output occurs.

Surprisingly, no significant difference was seen in the optical spectrum of the laser output between the pulsing and CW regimes. The only exception was in a low-power CW Raman-only regime, found with the pump up to 100 mW above threshold, although there is variation and apparent hysteresis in the Brillouin threshold. Figure 6 shows the response above this threshold, where it can be seen that not only does the Brillouin clamp the Raman output, it also reduces the output Raman power as pump power increases. This reduction in Raman output quickly leads to the Brillouin becoming the dominant laser output of the system. The spacing between Brillouin and Raman peaks of 12.7 GHz is as expected for this fiber and is consistent with that previously reported for UHNA4, but as the OSA is resolution limited this exact shift was not further investigated.

Using a ADVANTEST R3273 spectrum analyzer (100 Hz–26.51 GHz) the beat frequency between the Raman and Brillouin peaks was directly measured. Figure 7 shows the measured 12.8 GHz peak for both CW and pulsed lasing, confirming the OSA measurement. The peak width was limited by the 1 MHz bandwidth of the scan, which was found to be the smallest bandwidth that could reliably capture the beat frequency since it wandered on a sub-second time scale over approximately 5 MHz. Although narrower still bandwidth-limited peaks were

Optics EXPRESS

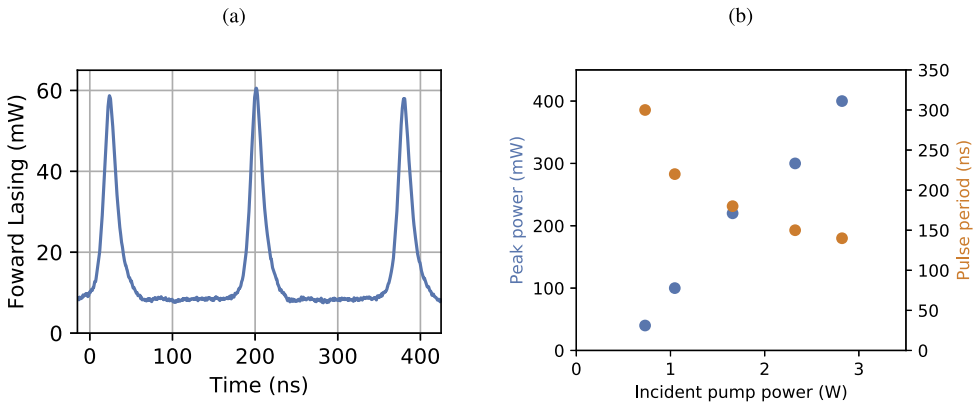

Fig. 4. (a) A typical example of pulsing output. (b) A response to pump power in both peak power (blue, left axis) and decreasing pulse period (orange, right axis).

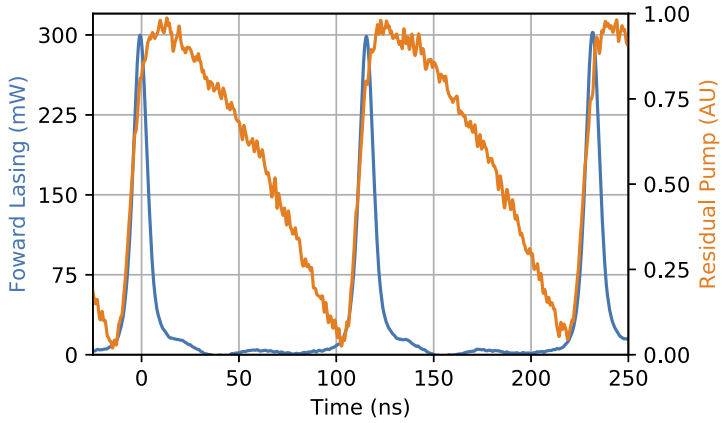

Fig. 5. Time trace of both the pulsed forward output (blue, left axis, DC coupled detector) and residual pump power (orange, right axis, AC coupled detector) at 2.25 W of incident pump power. Note that the AC coupled residual pump power trace corresponds to an approx. 5 % drop in power throughput.

seen in lower bandwidth scans, e.g. 10 kHz/1 kHz, these could not be reliably captured with the spectrum analyzer available. This gives a reasonable upper bound of 1 MHz for the 3 dB bandwidth of the beat frequency, implying that the Brillouin and Raman outputs are highly correlated; as the Raman signal has been reported by others as both SF and featuring ultra-narrow linewidths [16,17], the Brillouin signal must be as well. The pulsed spectrum also appears close to being bandwidth-limited by the scan, however, with greater noise and sidebands present, this cannot be said with absolute certainty. The pulsed spectrum is narrow enough to determine that the pulsed lasing is essentially single frequency, and not overly broadened, potentially near-transform-limited.

Optics EXPRESS

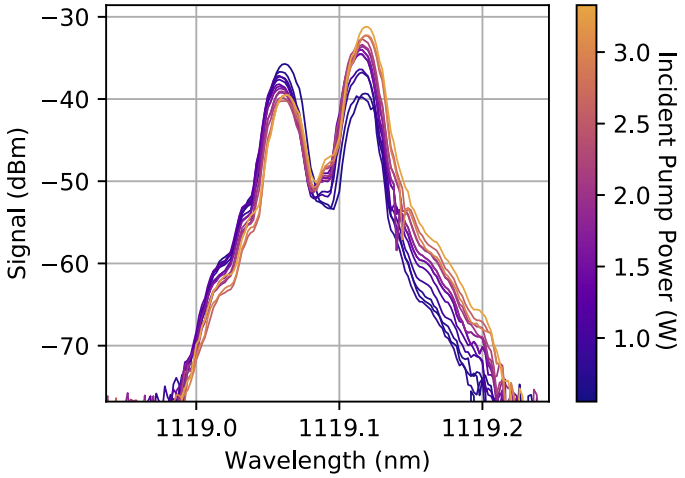

Fig. 6. Forward lasing spectral response to increasing pump power as measured by an OSA with no correction made for coupling losses between the laser and the OSA.

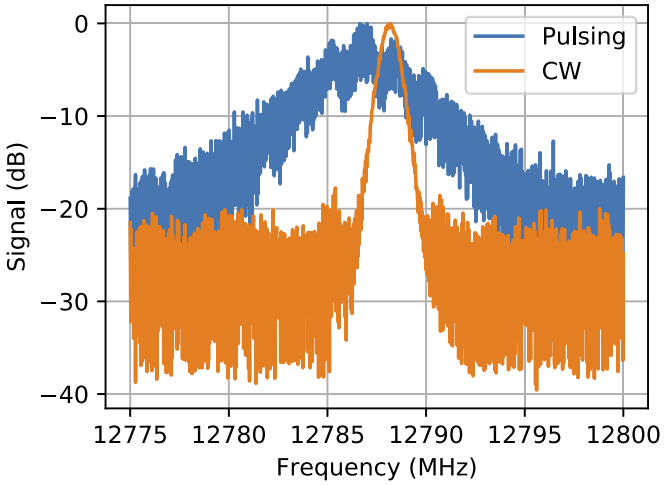

Fig. 7. Normalised beat frequency between the Raman and the Brillouin output, with a measurement bandwidth of 1 MHz.

5. Theory

In this section we consider a simple phenomenological model for the Raman laser similar in spirit to that used for Q-switched lasers [32,33]. We start by defining $R(t)$ as the total energy (measured in Joules) inside the cavity in the Raman mode at time t while $B(t)$ is the corresponding total energy of the light at the Brillouin frequency. Then

$$\frac{\mathrm{d}R}{\mathrm{dt}} = \text{Gain} - \text{Loss}, \tag{1}$$

with the expressions for the gain and loss terms still to be determined. We make the assumption that the longitudinal modes of the cavity do not change with time and thus, for example, the forward propagating electric field intensity at the Raman frequency is given by $I_r^+ = R/2M_R(z)$ with an identical expression for the backward propagating field since for the high Q cavities

Optics EXPRESS

considered here the energy is split equally. Here, $M_R(z)$ is the envelope obtained by solving the usual coupled mode equations for a π phase-shifted Bragg grating [7,10,16,34]. The Raman gain $G_r(z)$ at each point in the grating is given by the usual formula $G_r(z) = 2g_r' P(z) I_r^+(z)$ [35] where g_r' is the Raman gain coefficient for the material and $P(z)$ is the pump distribution assumed equal to $PM_p(z)$ where again P is the energy at the pump frequency in the fibre and M_p the intensity distribution along its length. The factor of two arises since the forward and backward propagating light see the same gain. The total gain is then the integral over the length of the fiber times the effective area of the mode (A_{eff}), i.e.

$$\text{Gain} = g_r' PR(t) A_{\text{eff}} \int_0^L M_P(z) M_R(z) \mathrm{d}z \quad = g_r PR(t), \tag{2}$$

where $M_P(z)$ is the profile of the pump beam while P represents its power. The cavity Raman gain g_r is thus given by the product of the overlap integral, the effective area (A_{eff}) and the usual Raman gain g_r' and has units of $1/(sJ)$.

The loss for the Raman mode comprises two terms. Firstly, there is a linear loss given by $\alpha_r R$ which comprises both the intrinsic fiber loss (which can be neglected for such small cavities and weak gratings) and the cavity loss, which can be calculated from the Q-factor of the Bragg grating. More importantly, there is a nonlinear loss term due to the Brillouin interaction which depends on the stored energy. Note that although the Brillouin is counterprogating compared to the Raman signal, the fact that the forward and backward propagating fields are essentially equal implies that there will be equal Brillouin gain in each direction as well. Thus, the cavity loss can be written as:

$$\begin{aligned} \text{Loss} &= g_b' R(t) B(t) A_{\text{eff}} \int_0^L M_B(z) M_R(z) dz + \alpha_r R(t) \\ &= g_b R(t) B(t) + \alpha_r R(t). \end{aligned} \tag{3}$$

Where g_b' is the usual Brillouin gain as defined in [35] and g_b the normalised cavity gain. We can also similarly derive an equation for the Brillouin energy giving us the final set of equations

$$\frac{\mathrm{d}R}{\mathrm{d}t} = g_r PR - g_b RB - \alpha_r R, \tag{4a}$$

$$\frac{\mathrm{d}B}{\mathrm{d}t} = g_b RB - \alpha_b B. \tag{4b}$$

Where α_b is the linear cavity loss at the Brillouin frequency defined in a similar manner to α_R. Eqs. (4) describe the evolution of energy stored inside the fibre grating which is not immediately observable since we can only measure the output power from the cavity which is given by $\alpha_r R(t) + \alpha_b B(t)$ and since for high Q cavities $\alpha_r \ll \alpha_b$ most of the light is actually emitted by the Brillouin signal. Although this is a simple model, it does however reproduce many of the main features of the physical system and can thus be used to aid our understanding as discussed below.

Firstly we can consider the predicted CW powers which correspond to the fixed points of Eqs. (4). In addition to the trivial fixed point, ($R = B = 0$), Eqs. (4) have a second fixed point given by

$$R = \frac{\alpha_b}{g_b} \quad \text{and} \quad B = \frac{g_r P - \alpha_r}{g_b}. \tag{5}$$

Thus, in our simple model for pump powers below $P = \alpha_r/g_r$ the lasing output will be zero and then it will jump discontinuously to the second fixed point after which the output will increase linearly and indeed this can be seen in Fig. 3. If the output power is resolved spectrally then the distinguishing feature of this fixed point is that the Raman energy is fixed while the Brillouin energy increases linearly with pump power. Experimentally, this has been observed by Loranger *et al.* when looking at the output spectrum [14] as well as ourselves (see Fig. 6). In Fig. 6 we

Optics EXPRESS

can see that this prediction is only approximately correct since there is a small decrease in the power at the Raman wavelength as the pump power increases, while the Brillouin power level increases significantly.

Secondly, the equations have a conserved quantity K given by

$$K = B^{g_r P - \alpha_R} R^{\alpha_b} e^{-g_b(R+B)} \tag{6}$$

which organises the dynamics of the system. Importantly, for each value of K the solution forms a closed loop in the $R-B$ plane as shown in Fig. 8 with the loops centred on the fixed point given by Eq. (5). We emphasise that each of the trajectories in Fig. 8 correspond to solutions with the same values of the parameters including the pump power and thus are all in principle observable. For all of our simulations below we set $g_r = 1$, $g_b = 10.0$, $\alpha_r = 0.02$, $\alpha_b = 30$ and a pump power $P = 12$ (discussed below in more detail). In Fig. 8 the black contours show equally spaced values of $log(K)$ which varies between -8 and -100 with higher values being nearer to the fixed point.

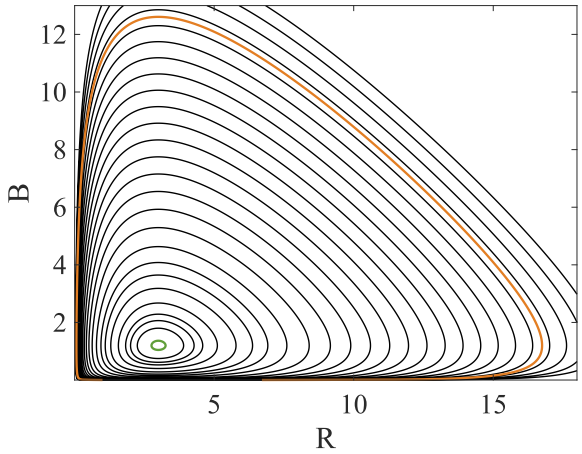

Fig. 8. Contour plot of the solutions to Eqs. (4) in the $R-B$ plane. Each contour corresponds to a different value of the integration constant K. In particular the green contour has a log(K) value of -6.96 while for the orange contour log(K)=-92.7.

The existence of the conserved quantity K means that the fixed point given in Eq. (5) is a neutral equilibrium and thus if the system is perturbed away from the fixed point, then we expect it to oscillate with a period depending on the distance from the fixed point. We show in Fig. 9 the expected stored energy and output time traces for small (green contour) and large (orange contour) oscillations in Fig. 8. This model also implies that the system is multi-stable for all pump values above threshold and can thus be switched from one oscillation mode to another due to the presence of noise. It is also especially sensitive to noise when $R \approx B \approx 0$ since all trajectories have to pass between the fixed point and the origin.

The time traces for the large oscillations (Fig. 9 bottom panels) correspond to what we refer to as Raman-Brillouin pulsing; this matches well the conceptual description given above since we can clearly see the slow buildup of stored energy at Raman frequency in the cavity (blue trace) which then is rapidly depleted as the Brillouin energy increases (orange trace). If these frequencies are not spectrally separated at the output, then the combined output will look like the right-hand traces in Fig. 9 as is the case for the current experimental setup.

For the traces and contours, the parameters chosen were $g_r = 1$, $g_b = 10.0$, $\alpha_r = 0.02$, $\alpha_b = 30$ and a pump power $P = 12$. These values are representative of realistic values similar to those used in the experimental results presented below. However, there is considerable uncertainty in them due to the unknown value of the overlap integrals in (2) and (3). So while the intrinsic

Optics EXPRESS

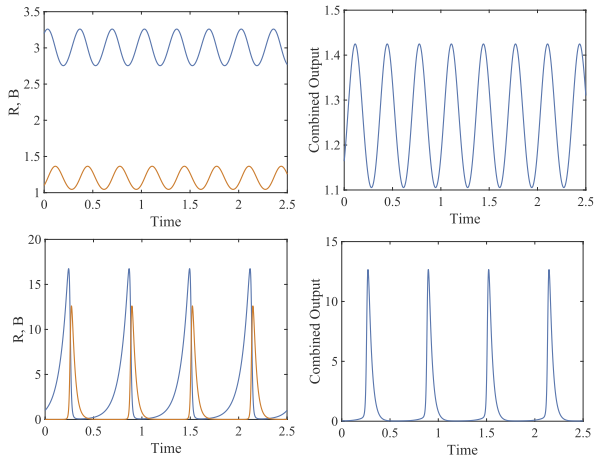

Fig. 9. Time traces corresponding to small and large oscillations. The Figs. on the left show the stored energy inside the cavity at the Raman (blue line) and Brillouin (orange) frequencies while those on the right show the combined output. The top trace corresponds to the green contour in Fig. 8 and shows small oscillations around the fixed point. The bottom trace corresponds to the orange contour in Fig. 8 and shows large oscillations around the fixed point. The time here is in units of the rise time for the Raman mode when $P = 1$.

Brillouin gain is nearly 1000 greater than the peak Raman gain in silica [35] the longitudinal mode profiles can change the value of g_r/g_b substantially. We have also estimated that the Raman signal is significantly better confined than the Brillouin signal and again this could easily vary by several orders of magnitude depending on the precise structure of the grating and any apodisation profile applied. In Fig. 6 if we assume that the Raman line is centred at the peak reflectivity then the Brillouin line would have a reflectivity of 2dB. However, the precise value depends critically on the fine details of the grating which we are unable to resolve. Eqs. (4) can be scaled so that any particular parameter is equal to unity, provided that time is also rescaled and we have adopted here the scaling that $g_r = 1$ and so time is measured in terms of the characteristic rise time for the Raman signal when $P = 1$. We can similarly set a second parameter to equal unity by an appropriate rescaling of the amplitudes(e.g $R \rightarrow \kappa R$) which again does not change the dynamics. What is then critical is the relative sizes of the coefficients since this determines the position of the fixed point given by Eq. (5) and the pump threshold for lasing. Importantly for our model, the dynamics remains the same for all parameter values with the only significant difference being the required pump power needed to reach threshold. Estimating this threshold would require a sufficiently detailed knowledge of the Bragg grating to allow us to calculate the overlap integrals, something which is not currently possible to do with any accuracy. Instead, we have thus chosen representative values for the parameters that clearly show the range of dynamical behaviour.

In deriving Eqs. (4), we assumed that the pump intensity profile $M_p(z)$ does not change with incident pump power or time. Experimentally, we have found that the residual pump power (i.e. $M_p(L)$) varies by less than 5% during the Q-switching cycle [see Fig. 5], and so this assumption is reasonable. However, the change in residual pump power can be used as a proxy for the stored Raman energy in the cavity and so can provide an estimate of $R(t)$ while the combined output can measured directly giving $B(t)$. Measuring the residual pump power as a function of time would then be expected to give a curve similar to $R(t)$ only inverted. This can be seen in Fig. 5 where the orange line is the residual pump and it behaves very similarly to what we expect from the theory. Another assumption going into our model is that the linear loss α_R of the Raman cavity does not change with time. In a real system α_R depends on the grating and in particular

Optics EXPRESS

the phase shift. Thermal effects are likely to change this for instance, however, such effects occur on a much slower timescale than the pulsing and so can be neglected in this simple model. In addition, at higher intensity (i.e. when the stored energy becomes large) Kerr effects could play a role in detuning the mode from the resonance, leading to a rapidly changing cavity loss. However, the intensities at which this happens are much higher than the threshold for Brillouin effects and again can be neglected to lowest order.

6. Discussion

In standard optical fiber, the usual threshold condition for Brillouin is given as $g_b(\Omega_b)P_{cr}L_{\text{eff}}/A_{\text{eff}} \approx 21$ [35] and so it is worth considering how this is exceeded in our cavity. Firstly, the high finesse of the grating means that the Raman light has a narrow linewidth (<2.5 kHz [13]) and so the Brillouin gain is as high as possible. Secondly, a small core fiber was used, decreasing A_{eff} significantly compared to normal fibers. Finally, unlike in normal fibers, the Brillouin light could be seeded by spontaneous Raman scattering in the forward direction, which is then amplified by the backwards propagating Raman light, further reducing the threshold. There are a few obvious improvements that can be made to this laser, such as moving to the peak of the Raman gain and increasing the reflectively of the cavity to improve the finesse. This would reduce the lasing threshold without compromising the slope efficiency as the outcoupling mechanism of the laser cavity is the Brillouin scattering, not the Raman lasing; however, the current cavity is already sufficiently reflective as to make measuring the cavity finesse difficult. There are questions around how moving the π-phase will effect the Brillouin lasing, but biasing the cavity toward one end of the grating will allow for biasing one or both of the output mechanisms in a preferred direction. In our model moving the phase shift would not change anything significantly with the only difference being that the gain would be a sum of two overlap integrals (for the forward and backward propagating fields respectively) and while more complicated this would not alter the dynamics in any way.

There are more intriguing aspects to this laser, such as the chaotic behaviour sometimes seen above certain power thresholds with evidence of bifurcation seen before this occurs. High frequency (GHz) pulsing has also been observed, both by itself and modulating the Q-switch-like pulsing. Degenerate four-wave mixing was found between the pump and Raman, and (at higher powers) pump and Brillouin waves at 1179.8 nm although with orders of magnitude less power than the lasing output. The laser's peak power was improved by placing a twenty gram weight one quarter the way along the copper mounting bar, with an increase in the peak pulse power from the 300 mW seen in Fig. 5 to 1200 mW produced. This is presumably due to the weight causing subtle distortions in the grating spectrum.

7. Conclusion

In conclusion, we have above demonstrated a new compact Raman-Brillouin laser based on π-phase DFB FBG cavity at 1119 nm, where the Brillouin Stokes shift is used as the primary output–coupling mechanism. This laser has a low pump threshold of 350 mW, a high slope efficiency of up to 14 %, and 250 mW output power with single-frequency operation in both CW and pulsed regimes. The pulsed regimes have been demonstrated to be SBS induces passive Q-switching/cavity dumping producing 20 ns pulse widths, repetition rates up to 10MHz, and typical peak pulse powers of 300 mW with 1200 mW possible. However, there are instabilities at higher powers as well as other effects such higher oscillations. Further work needs to be done to determine if the Brillouin is free running or has significant cavity enhancement, as well as work to either suppress or separate the Raman lasing from the Brillouin lasing.

In order to explain our experimental results, we have presented a simple phenomenological model that has the same key features as seen in the experiment, i.e. above threshold the power is increasingly emitted by the Brillouin signal and the co-existence of both stable and Q-switching

Optics EXPRESS

modes of operation. Note that there are several key assumptions in deriving Eq. (4). The first is that both the Brillouin and Raman signals are single frequency and single mode. Experimentally, the linewidth of the output of such lasers has been measured to be sub kHz [16,17] and so this is a reasonable assumption (although there is evidence that at high powers the DBR becomes multi-moded). We have also assumed that neither the mode shape or the pump power P changes with time. Experimentally, we measured a less than 5 % change in the output pump power and so this again is reasonable. The biggest error in our model is thus likely to arise from a change in the mode shape as the stored energy increases due to either thermal heating effects (which are slow) or the Kerr non-linearity (which is fast) and both of these effects would also change the cavity loss α_R. Nevertheless our simple model does explain many of the observed experimental features. Finally we note that our model, Eqs. (4), is identical to the well-known Lotka-Volterra predatory-prey model [36].

Funding. Innovate UK (104613, 50414); Engineering and Physical Sciences Research Council (EP/M024539/1, EP/T00097X/1); Royal Academy of Engineering.

Acknowledgments. Corin Gawith's role in this project was supported by the Royal Academy of Engineering under the Research Chairs and Senior Research Fellowships scheme.

Disclosures. The authors declare that they have no conflicts of interest.

Data Availability. The data from this paper can be obtained from the University of Southampton repository: [37].

References

1. J. T. Kringlebotn, J.-L. Archambault, L. Reekie, and D. N. Payne, "Er^{3+}:Yb^{3+}-codoped fiber distributed-feedback laser," Opt. Lett. **19**(24), 2101–2103 (1994).
2. W. H. Loh and R. I. Laming, "1.55 μm phase-shifted distributed feedback fibre laser," Electron. Lett. **31**(17), 1440–1442 (1995).
3. S. Vasilyev, A. Nevsky, I. Ernsting, M. Hansen, J. Shen, and S. Schiller, "Compact all-solid-state continuous-wave single-frequency UV source with frequency stabilization for laser cooling of Be^+ ions," Appl. Phys. B **103**(1), 27–33 (2011).
4. S. S. Sané, S. Bennetts, J. E. Debs, C. C. N. Kuhn, G. D. McDonald, P. A. Altin, J. D. Close, and N. P. Robins, "11 W narrow linewidth laser source at 780 nm for laser cooling and manipulation of rubidium," Opt. Express **20**(8), 8915–8919 (2012).
5. A. I. Lvovsky, B. C. Sanders, and W. Tittel, "Optical quantum memory," Nat. Photonics **3**(12), 706–714 (2009).
6. M. P. Hedges, J. J. Longdell, Y. Li, and M. J. Sellars, "Efficient quantum memory for light," Nature **465**(7301), 1052–1056 (2010).
7. Y. Feng, *Raman Fiber Lasers, Springer Series in Optical Sciences* (Springer International Publishing, 2017).
8. Y. Liu, J. Liu, and W. Chen, "Eye-safe, single-frequency pulsed all-fiber laser for doppler wind lidar," Chin. Opt. Lett. **9**(9), 090604 (2011).
9. G. W. Ross, M. Pollnau, P. G. R. Smith, W. A. Clarkson, P. E. Britton, and D. C. Hanna, "Generation of high-power blue light in periodically poled $LiNbO_3$," Opt. Lett. **23**(3), 171–173 (1998).
10. Y. Hu and N. G. Broderick, "Improved design of a DFB Raman fibre laser," Opt. Commun. **282**(16), 3356–3359 (2009).
11. P. S. Westbrook, K. S. Abedin, J. W. Nicholson, T. Kremp, and J. Porque, "Raman fiber distributed feedback lasers," Opt. Lett. **36**(15), 2895–2897 (2011).
12. J. Shi, S. ul Alam, and M. Ibsen, "Highly efficient Raman distributed feedback fibre lasers," Opt. Express **20**(5), 5082–5091 (2012).
13. J. Shi, S. ul Alam, and M. Ibsen, "Sub-watt threshold, kilohertz-linewidth Raman distributed-feedback fiber laser," Opt. Lett. **37**(9), 1544–1546 (2012).
14. S. Loranger, V. Karpov, G. W. Schinn, and R. Kashyap, "Single-frequency low-threshold linearly polarized DFB Raman fiber lasers," Opt. Lett. **42**(19), 3864–3867 (2017).
15. S. Loranger and R. Kashyap, "Efficiency increase of distributed feedback Raman fiber lasers by dynamic control of the phase shift," Opt. Lett. **43**(23), 5705–5708 (2018).
16. S. Loranger, A. Tehranchi, H. Winful, and R. Kashyap, "Realization and optimization of phase-shifted distributed feedback fiber Bragg grating Raman lasers," Optica **5**(3), 295–302 (2018).
17. J. Shi, "Periodic fibre devices for advanced applications in all-optical systems," Ph.D. thesis, University of Southampton (2012).
18. V. Karpov, S. Loranger, and R. Kashyap, "A tunable, single frequency, linearly polarized dfb raman fiber laser operating at 1178-nm," in *Advanced Photonics 2018 (BGPP, IPR, NP, NOMA, Sensors, Networks, SPPCom, SOF)*, (Optical Society of America, 2018), p. BW4A.2.

Optics EXPRESS

19. S. Loranger, V. Lambin-Iezzi, M. Wahbeh, and R. Kashyap, "Stimulated Brillouin scattering in ultra-long distributed feedback Bragg gratings in standard optical fiber," Opt. Lett. **41**(8), 1797–1800 (2016).
20. K. S. Abedin, P. S. Westbrook, J. W. Nicholson, J. Porque, T. Kremp, and X. Liu, "Single-frequency Brillouin distributed feedback fiber laser," Opt. Lett. **37**(4), 605–607 (2012).
21. D. Pohl, "A new laser Q-switch-technique using stimulated Brillouin scattering," Phys. Lett. A **24**(4), 239–240 (1967).
22. R. G. Harrison, J. S. Uppal, A. Johnstone, and J. V. Moloney, "Evidence of chaotic stimulated Brillouin scattering in optical fibers," Phys. Rev. Lett. **65**(2), 167–170 (1990).
23. R. G. Harrison, P. M. Ripley, and W. Lu, "Observation and characterization of deterministic chaos in stimulated Brillouin scattering with weak feedback," Phys. Rev. A **49**(1), R24–R27 (1994).
24. S. V. Chernikov, Y. Zhu, J. R. Taylor, and V. P. Gapontsev, "Supercontinuum self-Q-switched ytterbium fiber laser," Opt. Lett. **22**(5), 298–300 (1997).
25. M. Salhi, A. Hideur, T. Chartier, M. Brunel, G. Martel, C. Ozkul, and F. Sanchez, "Evidence of Brillouin scattering in an ytterbium-doped double-clad fiber laser," Opt. Lett. **27**(15), 1294–1296 (2002).
26. A. V. Kir'yanov, Y. O. Barmenkov, and M. V. Andres, "An experimental analysis of self-Q-switching via stimulated Brillouin scattering in an ytterbium doped fiber laser," Laser Phys. Lett. **10**(5), 055112 (2013).
27. F. Qamar and T. King, "Self pulsations and self Q-switching in Ho^{3+}, Pr^{3+}:ZBLAN fibre lasers at 2.87 μm," Appl. Phys. B **81**(6), 821–826 (2005).
28. X. Wang, H. Lv, P. Zhou, W. Wu, X. Wang, H. Xiao, and Z. Liu, "Single-frequency pulsed Brillouin-thulium fiber laser at 2 μm with nonlinear polarization rotation and active phase modulation," Appl. Phys. Express **7**(10), 102701 (2014).
29. L. Zhang, C. Wang, Z. Li, Y. Xu, B. Saxena, S. Gao, L. Chen, and X. Bao, "High-efficiency Brillouin random fiber laser using all-polarization maintaining ring cavity," Opt. Express **25**(10), 11306–11314 (2017).
30. Y. O. Barmenkov, P. Muniz-Cánovas, A. V. Kir'yanov, A. A. Carrascosa, J. L. Cruz, and M. V. Andrés, "Coexistence of Quasi-CW and SBS-Boosted Self-Q-Switched Pulsing in Ytterbium-Doped Fiber Laser With Low Q-Factor Cavity," J. Lightwave Technol. **38**(14), 3751–3758 (2020).
31. S. L. Scholl, A. Jantzen, R. H. S. Bannerman, P. C. Gow, D. H. Smith, J. C. Gates, L. J. Boyd, P. G. R. Smith, and C. Holmes, "Thermal approach to classifying sequentially written fiber Bragg gratings," Opt. Lett. **44**(3), 703–706 (2019).
32. O. Svelto, *Principles of Lasers* (Springer, New York, 2010), 5th ed.
33. M. Yamada, "A Theoretical-Analysis of Self-Sustained Pulsation Phenomena in Narrow-Stripe Semiconductor-Lasers," IEEE J. Quantum Electron. **29**(5), 1330–1336 (1993).
34. V. Perlin and H. Winful, "Distributed feedback fiber raman laser," IEEE J. Quantum Electron. **37**(1), 38–47 (2001).
35. G. Agrawal, *Nonlinear Fiber Optics, Optics and Photonics* (Elsevier Science, 2013).
36. P. J. Wangersky, "Lotka-volterra population models," Annu. Rev. Ecol. Syst. **9**(1), 189–218 (1978).
37. R. Bannerman, "Passively q-switching brillouin-raman distributed-feedback fiber hybrid laser," (2022). Available at https://doi.org/10.5258/SOTON/D2103.